4 SCIENTIFIC HIGHLIGHT OF THE MONTH

First-principles DFT+U study of radiation damage in UO_2: f electron correlations and the local energy minima issue

Michel Freyss[1], Boris Dorado[1,2], Marjorie Bertolus[1], Gérald Jomard[1], Emerson Vathonne[1], Philippe Garcia[1], Bernard Amadon[2]

[1] CEA, DEN, Centre de Cadarache, DEC/SESC/LLCC, 13108 Saint-Paul lez Durance, France

[2] CEA, DAM, DIF, 91297 Arpajon, France

Abstract

The present highlight reviews recent advances in first-principles modelling of radiation damage in UO_2. It focuses on the influence of strong correlations and the problem of metastable states that occur with some approximations that localize electrons, in particular the density functional theory (DFT)+U approximation. It gives an illustration that DFT+U calculations quantitatively describe atomic transport phenomena in strongly-correlated uranium dioxide, provided that one circumvents the DFT+U local energy minima issue that affects f-electron systems. The occupation matrix control (OMC) scheme is one of the techniques developed to tackle the metastable state issue. We demonstrate here its efficiency on perfect and defective UO_2 through the study of oxygen diffusion. We use OMC to calculate UO_2 bulk properties, defect formation energies, migration energy barriers, and we show that in order to avoid the metastable states and systematically reach the ground state of uranium dioxide with DFT+U, the monitoring of occupation matrices of the correlated orbitals on which the Hubbard term is applied is crucial. The presence of metastable states can induce significant differences in the calculated total energies, which explains the origin of the discrepancies in the results obtained by various authors on crystalline and defect-containing UO_2. Also, for the bulk fluorite structure of UO_2, we show that the widely used Dudarev approach of the DFT+U systematically yields the first metastable state when no control is done on the orbital occupancies. As for oxygen diffusion, the calculated migration energy relating to the interstitialcy mechanism compares very favourably to experimental data. Also, vacancy migration and Frenkel pair formation energies are shown to agree well with existing data.

1 Introduction

Uranium dioxide is the standard nuclear fuel used in pressurized water reactors and has been extensively studied during the last decades, both experimentally [1–8] and computationally [9–23]. In order to better understand the behaviour of this material under irradiation and in particular to gain some insight into point defect formation and migration, its accurate description by first-principles methods is necessary. Such a description, however, remains challenging. Previous

first-principles calculations [9–11] based on the density functional theory [24, 25] in the local density approximation (LDA) and in the generalized gradient approximation (GGA) failed to capture the strong correlations between the $5f$ electrons of uranium entirely. Within these two approximations, uranium dioxide is found to be a ferromagnetic metallic compound while it is actually an antiferromagnetic Mott-Hubbard insulator below 30 K. It is only with the development of approximations such as hybrid functionals for exchange and correlation [18, 26, 27], self-interaction correction (SIC) [16, 28] or approximations based on the addition of a Hubbard term to the Hamiltonian, such as DFT+U [29–31] and DFT+DMFT [32, 33], that the strong correlations between the $5f$ electrons of UO_2 could be better described.

Furthermore, the increase in available computing power enabled the study of large UO_2 supercells and with it the investigation of the formation and migration energies of point defects [15, 19, 22, 23, 34–36] and of the incorporation of fission products [37–41], mainly xenon, iodine, strontium, barium, zirconium, molybdenum and caesium, and of helium [42, 43]. These studies are of prime importance to better understand the behaviour of UO_2 under irradiation. Resulting migration energies can be used as input data in higher scale models (classical molecular dynamics, kinetic Monte Carlo simulations, rate theory...) and should therefore be calculated with high accuracy. Up to now, the large UO_2 supercells that are required to perform these calculations, containing around one hundred atoms, can only be studied using the DFT+U method because calculations using hybrid functionals or DFT+DMFT are still computationally prohibitive.

Unfortunately, significant discrepancies were observed in the formation and migration energies of point defects calculated at the DFT+U level and published in recent years, although the same method, the projector augmented-wave (PAW) method, and very similar calculation parameters were used. By a study of perfect UO_2 crystal [17], we were able to show that these discrepancies stemmed from the use of the DFT+U approximation. This formalism localizes the $5f$ electrons and creates numerous local energy minima (or metastable states), which makes it difficult to find the ground state of the system (see Sect. 2). Unlike the LDA or GGA approximations, the DFT+U formalism creates an orbital anisotropy that increases the number of metastable states, and consequently, the final state reached by the self-consistent algorithm and its associated total energy may be different depending on the starting point of the calculation (initial lattice parameter, initial uranium magnetic moments, etc). The DFT+U method is based on the Hartree Fock (HF) approximation. The latter has been known to exhibit such multiple solutions for a long time [44, 45]. This increased number of energy minima has also been observed in UO_2 within other approximations that localize electrons, such as hybrid functionals [36], as well as in other $4f$ and $5f$-compounds such as γ-Ce [46, 47], PrO_2 [48], PuO_2 [49] and rare earth nitrides [50]. The DFT+U study on cerium by Amadon *et al.* [47] in particular showed that the density matrix in the correlated subspace had to be monitored carefully, especially to study magnetism. Moreover, the work of Jomard *et al.* [49] on plutonium oxides PuO_2 and Pu_2O_3 provided a practical procedure which consists in comparing the energies of all energy minima and therefore allowed to unequivocally determine the ground state.

With a 96-atom UO_2 unit cell as typically used for the study point defects and impurities, the difference in the total energy between the ground state and metastable states can reach up to 3 eV. The existence of these metastable states therefore strongly affects the calculated formation energies of point defects and, as a consequence, any result derived from these formation energies:

concentration of defects, solubility of fission products, etc. It is therefore important to ensure that the ground state of the system has indeed been reached.

In this review, we report a detailled study of the ground state and metastable states of uranium dioxide obtained with DFT+U and investigate the influence of the metastable states on the structural and electronic properties of the material. We present the theoretical background for the DFT+U formalism and the orbital anisotropy it implies for the $5f$ orbitals. We show that if one wishes to reach the ground state systematically, the most effective method is to switch off all wave-function symmetries and to precondition the electronic occupancies of the $5f$ orbitals, i.e., to impose initial $5f$ electron occupation matrices and monitor them during the calculations. This so-called occupation matrix control scheme (OMC) is an alternative to more recent schemes developped to avoid metastable states in f-compounds: the U-ramping scheme [51] and the quasi-annealing scheme (QA) [52]. Using the DFT+U method with the OMC scheme, we have studied the stability of the Jahn-Teller (JT) distortion in UO_2 and calculated oxygen and uranium point-defect formation energies in both the fluorite and the Jahn-Teller distorted structures. Our results are compared with those from the literature and we discuss the discrepancies observed. Finally, the DFT+U results on the migration mechanisms and energies of oxygen ions in UO_2 are reported.

2 The DFT+U method and the local minima issue

2.1 The DFT+U method

Given the failure of standard density functional theory approximations (namely, the local density approximation LDA and the generalized gradient approximation GGA) to describe correctly uranium dioxide, we used the DFT+U approximation (*i.e.* the LDA+U or the GGA+U approximation) that improves the treatment of the correlations between the uranium $5f$ electrons. The DFT+U energy functional introduces a correction to the standard DFT energy functional given by

$$E^{\mathrm{DFT+U}} = E^{\mathrm{DFT}} + E_{\mathrm{Hub}} - E_{\mathrm{dc}}. \tag{1}$$

The first term E^{DFT} is the standard DFT (LDA or GGA) contribution to the energy. The second term E_{Hub} is the corrective electron-electron interaction term to account for the enhanced electron correlations and it takes a similar form as the U term of Hubbard model [53] in the static mean field approximation. E_{dc} is the double-counting correction. E_{Hub} and E_{dc} depend on the occupation matrices of the correlated orbitals.

There are various formulations of the DFT+U functionals. Although they can all be written in the form given in equation (1), they differ with the choice of

- the DFT exchange-correlation functional (LDA or GGA).
- the formulation of the Hubbard term E_{Hub} and the values of the U and J parameters contained in E_{Hub}.

- the double-counting term $E_{\rm dc}$.
- the Kohn-Sham orbital projection method used to calculate the electron occupancies. However, with equal U and J values and with the same double-counting term, two electron occupancy calculations using two different projection methods will give similar results [54].

The Hubbard term

We used the two currently available approaches to describe the Coulomb interaction Hubbard term $E_{\rm Hub}$. They were respectively introduced by Liechtenstein *et al.* [30] and Dudarev *et al.* [31]. The Hubbard interaction term is expressed in the following rotationally invariant form:

$$\begin{aligned} E_{\rm Hub}[n^I_{mm'}] &= \frac{1}{2}\sum_{\{m\},\sigma,I}\{\langle m,m''|V_{ee}|m',m'''\rangle n^{I\sigma}_{mm'}n^{I-\sigma}_{m''m'''} \\ &\quad +(\langle m,m''|V_{ee}|m',m'''\rangle - \langle m,m''|V_{ee}|m''',m'\rangle)n^{I\sigma}_{mm'}n^{I\sigma}_{m''m'''}\}, \end{aligned} \tag{2}$$

where $n^{I\sigma}_{mm'}$ is the occupation matrix on site I (see Sect. 2.1.1). $E_{\rm Hub}$ can be expressed as a function of the direct Coulomb U and exchange J interactions:

$$U = \frac{1}{(2l+1)^2}\sum_{m,m'}\langle m,m'|V_{ee}|m,m'\rangle \tag{3}$$

and

$$J = \frac{1}{2l(2l+1)}\sum_{m\neq m',m'}\langle m,m'|V_{ee}|m',m\rangle \tag{4}$$

The Dudarev approach is a simplified form of the Liechtenstein approach. It uses the difference $(U-J)$, contrary to the Liechtenstein approach in which the U and J terms come into play separately.

The double-counting term

The third term in Eq. (1), the double-counting term $E_{\rm dc}$, is not specific to the DFT+U formalism but is required in all methods that add a correlation term to the standard DFT functional. The double-counting term is aimed at substracting the LDA or GGA exchange-correlation contribution already counted in $E^{\rm DFT}$. There are several expressions for the double-counting term. In the so-called around mean field (AMF) approach, introduced by Czyżyk and Sawatzky [55], $E_{\rm dc}$ takes the following form:

$$E^{\rm AMF}_{\rm dc} = UN_\uparrow N_\downarrow + \frac{1}{2}\frac{2l}{2l+1}(U-J)\sum_\sigma N^2_\sigma, \tag{5}$$

where N is the total number of electrons, N_σ is the total number of electrons with spin σ ($\uparrow$ or $\downarrow$) and l is the quantum orbital number of the orbitals on which the DFT+U correction is applied.

In the fully localized limit approach (FLL), introduced by Anisimov *et al.* [56], the double-counting term is expressed as:

$$E_{\mathrm{dc}}^{\mathrm{FLL}} = \frac{1}{2}UN(N-1) - \frac{1}{2}J\sum_{\sigma}\left(N_{\sigma}^{2} - N_{\sigma}\right). \tag{6}$$

The main difference between the AMF and FLL double-counting terms is that the AMF tends to favor low spin configurations of the system whereas the FFL tends to favor high spin configurations [54]. In UO_2, the AMF and FLL approaches, however, yield the same results, i.e. a high spin configuration with a magnetic moment of $\pm 2\mu_{\mathrm{B}}$ on uranium cations.

2.1.1 Occupation matrices

Occupation matrices describe the electron occupancies of the correlated orbitals and play an important role in the DFT+U formalism (see Eq. (2)). An occupation matrix is defined as:

$$n_{m,m'}^{\sigma} = \sum_{n,\mathbf{k}} f_{n,\mathbf{k}}^{\sigma} \langle \psi_{n,\mathbf{k}}^{\sigma} | P_{m,m'} | \psi_{n,\mathbf{k}}^{\sigma} \rangle, \tag{7}$$

in which $\psi_{n,\mathbf{k}}^{\sigma}$ is a valence wave function corresponding to the state (n,$\mathbf{k}$) of spin σ and $f_{n,\mathbf{k}}^{\sigma}$ is the corresponding occupation number. $P_{m,m'}$ are projection operators on the localized orbitals. As an example, an occupation matrix for correlated $5f$ orbitals with spin up ($\uparrow$) takes the form:

$$n_{m,m'}^{\uparrow} = \begin{pmatrix} n_{-3,-3}^{\uparrow} & n_{-3,-2}^{\uparrow} & \cdots & \cdots & n_{-3,+3}^{\uparrow} \\ n_{-2,-3}^{\uparrow} & n_{-2,-2}^{\uparrow} & \ddots & & \vdots \\ \vdots & \ddots & \ddots & \ddots & \vdots \\ \vdots & & \ddots & n_{+2,+2}^{\uparrow} & n_{+2,+3}^{\uparrow} \\ n_{+3,-3}^{\uparrow} & \cdots & \cdots & n_{+3,+2}^{\uparrow} & n_{+3,+3}^{\uparrow} \end{pmatrix} \tag{8}$$

There is no unique way to define occupation matrices of localized atomic states [57]. In the present review, the occupation matrices were calculated in the basis of real spherical harmonics. The DFT+U formalism is rotationally invariant [30], which implies that it is always possible to find a basis in which the occupation matrix is diagonal.

2.2 The occurence of metastable states

In the DFT+U approximation, the strongly correlated electrons are localized on specific orbitals, contrary to standard DFT approximations which, in the case of UO_2, fill the orbitals with fractional electron occupancies. For this reason, with LDA and GGA, UO_2 is found metallic instead of insulator as it should be. The counterpart for this localization of the f electrons is the existence of various ways of filling the correlated orbitals, from which only one electron configuration corresponds to the ground state of the system. This leads to the existence of multiple local energy minima (or metastable states) in which calculations can get trapped because of the difficulty to go from one electron configuration to another. It is thus necessary to make sure that the ground state of the system is reached in all DFT+U calculations. In the case of

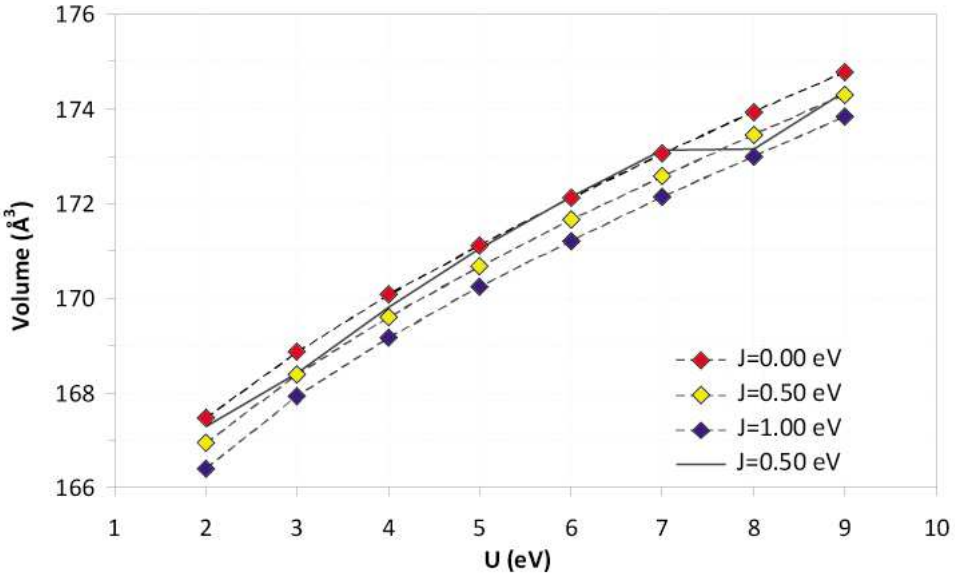

Figure 1: Variation of the 12-atom UO_2 supercell volume as a function of the U and J parameters of Liechtenstein DFT+U. The black line corresponds to the calculations from an arbitrary input wave function, in which the monitoring of the occupation matrices has not been performed.

bulk UO_2, the occurence of the metastable states is linked to the various possibilities for the two $5f$ electrons to occupy the seven $5f$ orbitals of the U^{4+} ions.

As can be easily experienced with DFT+U calculations even on the bulk UO_2 crystal, a DFT+U calculation starting from an arbitrary input wave function does not automatically converge to the lowest energy state. For instance, the convergence toward metastable states can be seen Fig. 1 which shows the variation of the UO_2 volume as a function of the U-parameter of the DFT+U method. The curve corresponding to the calculations from an arbitrary input wave function is rather erratic whereas the curves corresponding to the ground state of the crystal are perfectly smooth. Such a blunt illustration of the occurrence of metastable states can also be seen in Fig. 3 of the article by Jomard *et al.* for PuO_2 [49].

An efficient method to reach the ground state electronic configuration consists in testing several initial electron occupancies as a starting point of the calculation and determining the final occupancies that correspond to the lowest energy state. Such a scheme was used for the DFT+U study of several other correlated $4f$ and $5f$ compounds, such as cerium [46, 47], rare-earth nitrides [50] or plutonium oxides [49]. We have applied this method to UO_2. We defined initial input f electron occupation matrices and we imposed them during the calculation of the DFT+U potential. We thus preconditioned the calculation of the potential which was then applied as a correction to the standard DFT potential. Occupation matrices are imposed during the first 10 to 30 electronic steps, depending on the complexity of the system. After these initial constrained steps, the calculation is left to converge self-consistently on its own.

In order to determine the ground state occupancy of bulk UO_2, we imposed as a first step initial diagonal occupation matrices. There are $C_2^7 = 21$ different ways of filling the seven $5f$ levels with

Table 1: UO_2 states reached as a function of the initially imposed diagonal occupation matrices (defined by m_i and m_j) not taking into account the symmetries of the crystal and with Liechtenstein DFT+U. Δ is the UO_2 band gap. The lowest energy is fixed to zero.

i	j	Initial Matrix	$E - E_{\min}$ (eV / U_2O_4)	Δ (eV)
-3	-2	[1100000]	1.67	0.8
-3	-1	[1010000]	0.15	1.9
-3	0	[1001000]	0.01	2.5
-3	1	[1000100]	0.03	2.3
-3	2	[1000010]	0.07	2.5
-3	3	[1000001]	0.03	2.3
-2	-1	[0110000]	1.67	0.8
-2	0	[0101000]	1.72	0.9
-2	1	[0100100]	1.67	0.8
-2	2	[0100010]	2.68	0.2
-2	3	[0100001]	1.67	0.8
-1	0	[0011000]	0.00	2.4
-1	1	[0010100]	0.78	1.6
-1	2	[0010010]	0.07	2.5
-1	3	[0010001]	0.03	2.3
0	1	[0001100]	0.00	2.4
0	2	[0001010]	0.16	2.0
0	3	[0001001]	0.01	2.5
1	2	[0000110]	0.07	2.5
1	3	[0000101]	0.15	1.9
2	3	[0000011]	0.07	2.5

two electrons. Since there are several degenerate f levels, some of the electronic configurations are identical by symmetry. However, in order to check the consistency and the accuracy of the procedure, we did not take into account the f-level degeneracies and we studied all 21 electronic configurations. The imposed occupation matrices can be defined by the two quantum numbers m_i and m_j corresponding to the filled orbitals. As an example, the diagonal occupation matrix corresponding to occupied m_{-2} and m_3 orbitals will be noted [0100001].

Table 1 gives the energies of the UO_2 states reached as a function of the diagonal occupation matrices initially imposed, not taking into account the symmetries of the crystal. A study by Larson *et al.* [50] and our systematic study of UO_2 [17] indeed showed that keeping the crystal symmetries would hamper even more the convergence to the ground state. As a static mean field approximation, DFT+U (or Hartree Fock) indeed stabilizes symmetry-broken solutions [58]. Of course, lifting the symmetry results in a higher computational cost but is compensated by the accuracy of the result.

We see from Table 1 that ten states are reached depending on the starting electron occupation

configuration. The calculations with the initial occupation matrices [0001100] and [0011000] lead to the ground state of the UO_2 crystal. Several of the other final states are just few tenth of meV / UO_2 above the ground state but they can display electronic properties different from the ground state, as shown by the band gap values. When the symmetries of the crystal are kept, metallic states can even be obtained. Structural properties also exhibit slight differences, as will be shown in Sect. 3. The final $5f$ orbital occupation matrices obtained for the ground state of UO_2 (with the collinear $1\mathbf{k}$ antiferromagnetic order - see Sect. 3), using the Liechtenstein DFT+U and without symmetries, are reported below.

Spin ↑ component:

$$\begin{pmatrix} 0.61126 & 0.00000 & 0.44840 & -0.00058 & 0.00000 & -0.00039 & 0.00001 \\ 0.00000 & 0.11832 & 0.00000 & 0.00000 & -0.00001 & 0.00000 & 0.00000 \\ 0.44840 & 0.00000 & 0.37479 & -0.00004 & 0.00000 & -0.00060 & 0.00001 \\ -0.00058 & 0.00000 & -0.00004 & 0.64060 & 0.00008 & -0.44102 & -0.00002 \\ 0.00000 & -0.00001 & 0.00000 & 0.00008 & 0.02762 & -0.00006 & -0.00442 \\ -0.00039 & 0.00000 & -0.00060 & -0.44102 & -0.00006 & 0.35045 & 0.00002 \\ 0.00001 & 0.00000 & 0.00001 & -0.00002 & -0.00442 & 0.00002 & 0.03100 \end{pmatrix}$$

Spin ↓ component:

$$\begin{pmatrix} 0.03167 & 0.00000 & 0.00366 & 0.00000 & 0.00000 & 0.00000 & 0.00000 \\ 0.00000 & 0.09432 & 0.00000 & 0.00000 & 0.00000 & 0.00000 & 0.00000 \\ 0.00366 & 0.00000 & 0.02519 & 0.00000 & 0.00000 & 0.00000 & 0.00000 \\ 0.00000 & 0.00000 & 0.00000 & 0.02927 & 0.00000 & 0.00080 & 0.00000 \\ 0.00000 & 0.00000 & 0.00000 & 0.00000 & 0.02472 & 0.00000 & -0.00349 \\ 0.00000 & 0.00000 & 0.00000 & 0.00080 & 0.00000 & 0.02226 & 0.00000 \\ 0.00000 & 0.00000 & 0.00000 & 0.00000 & -0.00349 & 0.00000 & 0.02832 \end{pmatrix}$$

Note that the ground state occupation matrices have been determined by testing not only diagonal occupation matrices, but also numerous non diagonal ones. These matrices will be the input occupation matrices for all subsequent calculations of UO_2 supercells and will precondition the DFT+U calculations in order to avoid the convergence toward a metastable state. They were used for all calculations reported below on UO_2 bulk properties, as well as point defect formation and migration. This scheme was also used in the study of thermodynamic properties of UO_2 [59].

2.3 Methods developed to avoid metastable states

In order to perform accurate DFT+U calculations and make sure that the calculations converge to the ground state of the system, an *ad hoc* procedure has to be applied to avoid the convergence of the calculations to a local energy minima. Up to now, three procedures have been developed, including the one (OMC) used in the previous section and which we recall:

• The occupation matrix control scheme (OMC) [17]: It requires a systematic search of the ground state electronic configuration (in the form of the occupation matrices of the correlated orbitals) for the bulk perfect crystal. This ground state occupation matrix has to be imposed

at the beginning of subsequent calculations (for the first 10 to 30 electronic iterations) in order to precondition the convergence of the calculation toward the ground state. This procedure proved efficient for perfect bulk systems and systems with point defects or fission gases. The convergence to the ground state is also better ensured by switching off symmetries in order to lift degeneracies.

• The U-ramping scheme [51]: The Coulomb U parameter of the DFT+U method is slowly increased from 0 (standard DFT calculation) to its desired value, typically by steps of 0.1 eV. Results on the incorporation of rare gases in UO_2 [60] show that the U-ramping method is efficient on defective systems. The ground state of perfect bulk UO_2 could, however, not be reached using this method.

• The quasi-annealing scheme (QA) [52]: A fictitious fluctuation of the external potential is introduced, which is gradually suppressed in order to explore the potential surface. The results for the UO_2 perfect crystal are similar to the ones obtained with the occupation matrix scheme [61] (see below). For point defects or fission gas behaviour in UO_2, no comparison has been possible so far because of the different exchange-correlation functionals used (LDA+U vs. GGA+U).

A comparison was performed between the OMC and QA methods for a DFT+U calculation of the absolute total energy of the UO_2 crystal. The results are reported in Table 2 and show a small 10 meV / UO_2 difference between the OMC and the QA calculations. This discrepancy is not likely due to metastable states, but rather to a minor difference in calculation parameters. The 180 meV difference with the calculation using an arbitrary input wave function is, on the contrary, clearly due to the convergence to a metastable state. Up to now, only the QA approach has been proved as successful as the OMC scheme in reaching the ground state of bulk UO_2.

Table 2: Absolute DFT+U energy (eV/UO_2) of the UO_2 crystal calculated with the OMC scheme, the QA scheme and from an arbitrary input wave function, using otherwise the same calculation parameters [61].

	OMC	QA	arbitrary
Total energy (eV/U_4O_8)	-117.136	-117.095	-116.959

The main advantage of the OMC scheme is that when the ground state occupancy is known, one can perform calculations of supercells containing point defects or impurities without any increase of computational time. It is often argued that the OMC scheme requires numerous calculations in defective systems in order to find the ground state. This is not true if one can assume that the ground state occupation matrices of the perfect crystal can be used for the defective structure. Far from the defect, occupation matrices are not modified and are identical to those of the ground state. Close to the defect, on the contrary, the ground state occupation matrices will be quickly reoptimized into more complex electronic occupancies. In the end, the OMC scheme on defective supercell only requires one or a few calculations, depending whether near the defect cations with various oxidation states and different occupation matrices must be imposed (see Sect. 4.1). This is not the case with the U-ramping and QA methods in which the U parameter has to be slowly increased and the fluctuation of the external potential slowly removed, respectively. The OMC scheme is straightforwardly available in the ABINIT [62] code

and was implemented by our group in the VASP code.

2.4 Calculation parameters

All calculations reported here were carried out within the PAW formalism [63] for the calculation of the Kohn-Sham wave functions, as implemented in the VASP [64, 65] and ABINIT [62, 66] codes. For the exchange and correlation energy, we used the GGA functional as parametrized by Perdew, Burke, and Ernzerhof (PBE) [67]. The U and J values of the DFT+U approximation were set to 4.50 eV and 0.54 eV, respectively, as determined by Yamazaki and Kotani from the analysis of X-ray photoemission spectra [68, 69]. These values were kept constant in all calculations, whatever the defect considered. It is indeed *a priori* unnecessary to change these values once they have been defined for a given material: on the one hand, the U and J values in UO_2 mainly depend on the hybridization of uranium $5f$ and oxygen $2p$ orbitals, which is not significantly modified with the presence of a point defect in the material. Even if uranium ions around a point defect change their oxidation states (see Sect. 4.1), only a slight change in their local interaction U can be expected. For simplicity, we neglect these differences. On the other hand, U and J describe the Coulomb interaction between electrons that are located on the same atomic site, hence referred to as intra-atomic interactions. Given that the $5f$ electrons are strongly localized, it is unlikely that the presence of a defect would significantly change the very nature of these interactions.

For bulk calculations with a 12-atom UO_2 conventional cell, a 600 eV cut-off energy for the plane-wave basis set was used and a 6x6x6 Monkhorst-Pack for the sampling of the irreducible part of the Brillouin zone. For the 96-atom supercells, the cut-off energy was slightly reduced to 500 eV and a 2x2x2 Monkhorst-Pack was used. We add or remove oxygen or uranium atoms from this supercell to create either interstitial or vacancy point defects. The oxygen interstitial and vacancy induce a supercell volume variation of 0.3 % and 0.02 %, respectively. We can therefore consider that the supercell size is large enough to accommodate these defects. In all defect calculations, we used the collinear $1\mathbf{k}$ antiferromagnetic order as an approximation of the paramagnetic order of the UO_2 fluorite phase above 30 K. Moreover, we used a Gaussian smearing for fractional occupancies with a smearing width of 0.1 eV.

To determine the migration barriers, we used the CI-NEB (climbing-image nudged elastic band) method [70] as implemented in the VASP package. Since the determination of saddle points is efficient with only a small number of intermediate images along the reaction path, we used five images for the calculations of the minimum energy path.

In all calculations, spin-orbit coupling (SOC) was neglected. The inclusion of SOC causes drastic modifications in the occupation matrices of uranium atoms since it induces the filling of nondiagonal spin components that give rise to the orbital magnetic moment. Moreover, taking SOC into account significantly increases the number of metastable states since additional occupation matrices are to be considered, as a consequence of which a new systematic search for the ground state would have to be carried out. This, however, remains to be done to see the effect of SOC on defect formation and migration energies.

3 DFT+U results on bulk properties of UO_2

Above its Néel temperature of 30 K, UO_2 is paramagnetic and crystallizes in the fluorite structure (CaF_2): the uranium U^{4+} ions form a face-centred cubic sublattice while oxygen O^{2-} ions occupy the tetrahedral sites. Below 30 K, UO_2 is antiferromagnetic (AFM) and exhibits a static Jahn-Teller distortion of the oxygen sublattice [4, 71–74].

In fluorite UO_2, whose space group is $Fm\bar{3}m$, the point group of uranium is O_h and the crystalline field splits the seven $5f$ orbitals of the uranium atom into two threefold-degenerate levels (T_{1u} and T_{2u}) and one nondegenerate level (A_{2u}). As regards the antiferromagnetism in UO_2, experiments [3, 73, 75] and recent first-principles calculations [76] show that UO_2 has a non-collinear 3**k** antiferromagnetic order. However, due to the high computational cost, neither the non-collinear antiferromagnetism nor paramagnetism can be taken into account in point-defect calculations and we consider a collinear 1**k** antiferromagnetic order (also often referred to as the AFM1 or AFM(001) order), in which the spins of uranium atoms change sign along the Oz axis. This approximate 1**k** AFM order changes the point group of uranium from O_h to D_{4h}. In this case, the crystalline field splits the $5f$ orbitals into two twofold-degenerate levels (2 x E_u) and three nondegenerate levels (A_{2u}, B_{1u}, and B_{2u}).

The structural parameters and elastic constants are calculated for both the fluorite phase and the Jahn-Teller distorted phase, with a special attention to the magnetic ordering. In all cases, we imposed the appropriate occupation matrix at the beginning of the calculations to make sure that the lowest energy state is reached and that the results correspond to the ground state properties of the crystal in the structure considered.

3.1 The UO_2 fluorite phase

The structural parameters, bulk modulus and elastic constants of UO_2 in the fluorite phase are reported in Table 3.

Table 3: Lattice parameters (a, b, c), elastic constants (C_{11}, C_{12} et C_{44}) and bulk modulus (B) of UO_2 in the fluorite phase, calculated using Liechtenstein DFT+U.

	DFT+U	Experiments [77, 78]
Point group	D_{4h}	O_h
(a, b, c) (Å)	$5.57; 5.57; 5.49$	5.47
C_{11} (GPa)	346	389
C_{12} (GPa)	118	119
C_{44} (GPa)	58	60
B (GPa)	194	207

DFT+U structural parameters and elastic constants are in very good agreement with experimental values, despite the approximation on the magnetic ordering. The 1**k** antiferromagnetic order, however, causes a slight compression of the lattice along the z axis, which modifies the point group symmetry of uranium atoms. The T_{2u} levels of the O_h symmetry are split into an

occupied E_u level and an empty B_{2u} level in the D_{4h} symmetry. Since the doubly degenerate level E_u [$x(y^2 - z^2)$ and $y(z^2 - x^2)$] is oriented along the z axis, the compression occurs in this direction. We have also observed that in the first metastable state, the lattice is not compressed but expanded. With the Dudarev DFT+U, it is the other way around. The determination of the c/a ratio therefore constitutes a simple test to check if the ground state has been reached. Table 4 summarizes these results as a function of the DFT+U approaches used.

Table 4: c/a ratio of the UO_2 unit cell as a function of the state obtained and the DFT+U approximation used.

	Liechtenstein	Dudarev
Ground state	Compression	Dilatation
	$c/a = 0,99$	$c/a = 1,01$
1^{st} metastable state	Dilatation	Compression
	$c/a = 1,01$	$c/a = 0,99$

It should also be stressed that when occupation matrices are controlled, i.e. when the ground state is reached, the two DFT+U approaches yield similar electronic states: occupation matrices are identical, only the cell parameters differ (see Table 4). This is consistent with the fact that the Dudarev approach is a simplified version of the Liechtenstein approach. When occupation matrices are not controlled, however, calculations with the Dudarev approach do not reach the ground state. Instead, they reach the first metastable state, located 25 meV/UO_2 above the ground state.

3.2 The Jahn-Teller distortion

As mentioned before, below 30 K the oxygen sublattice displays a static Jahn-Teller distortion (JT) and the magnetic order is a non-collinear 3**k** AFM order [74]. The oxygen cage is distorted with an estimated displacement of oxygen atoms of 0.014 Å in the <111> directions, changing the space group from $Fm\bar{3}m$ to $Pa\bar{3}$ [74].

As a first step, the stability of the JT distortion was studied with an approximated 1**k** AFM order and compared to the fluorite structure with the same magnetic structure. Second, the relative stability of the 1**k** and 3**k** AFM orders were compared in the JT distorted phase (see Sect. 3.3).

In the study of the JT distorted structure, the oxygen atoms are located initially in the experimentally determined positions (space group: $Pa\bar{3}$). The lattice structure is then optimized and the total energy compared to that of the UO_2 ground state in the fluorite structure with a 1**k** AFM order. Our results indicate that the JT distortion stabilizes the lattice by 52 meV/UO_2, which is significant. Several calculations were done for the JT phase with various initial occupation matrices. All calculations converged to the same final state, emphasizing that when symmetries are broken, as induced by the oxygen atomic displacements, the DFT+U calculations reach the ground state more easily.

Despite the numerous studies of the AFM order in the JT phase, there are few experimental

data on the structural parameters of this phase. The elastic constants at 0 K can be determined by extrapolation of data from the 1967 study by Brandt and Walker [79]. In Table 5, we report the calculated and experimental lattice parameters, elastic constants and bulk modulus of UO_2 in the JT distorted phase.

Table 5: Lattice parameters (a, b, c), elastic constants (C_{11}, C_{12} and C_{44}) and bulk modulus (B) of uranium dioxide in the Jahn-Teller distorted phase with a 1**k**-antiferromagnetic order, calculated with the Dudarev DFT+U and compared to experiments.

	DFT+U	Experiments
(a, b, c) (Å)	5.054	–
C_{11} (GPa)	358	400
C_{12} (GPa)	109	126
C_{44} (GPa)	65	59
B (GPa)	192	217

The DFT+U values are in good agreement with the experimental data. The elastic constants of the JT phase are not very different from those in the fluorite phase. More significant is the result that the crystal lattice with the JT distortion remains cubic, which is not the case in the fluorite phase obtained using DFT+U (see Table 3). The oxygen sublattice distortion that we obtain corresponds to 0.09 Å displacements essentially in the $\langle 100 \rangle$ direction, which are, however, much too large compared to the ones reported from experiments (0.014 Å displacements in the $\langle 111 \rangle$ direction) [80]. The fact that the directions are different may be explained by our approximation of a collinear 1**k** AFM magnetic order instead of the 3**k** order.

In the JT 1**k** phase, the occupation matrices of all uranium atoms are identical and they only differ by the sign of some matrix elements. Those occupation matrices are noted OM_{JT} and will be subsequently used as initial occupation matrices for calculations with supercells containing point defects. Those results also show that in the perfect bulk crystal, the electron occupations of the uranium atoms are directly linked to the oxygen positions due to the fact that the oxygen atoms govern the crystal field applied to the uranium atoms. This crystal field modifies in return the point group symmetry at the uranium site, hence the $5f$ orbital degeneracies. In the 1**k** fluorite structure, the symmetry point group is D_{4h} and the crystal field imposes a particular form for the occupation matrices. When the oxygen cage is distorted, the point group symmetry becomes C_{3i} and the occupation matrices have a different form.

3.3 Non-collinear magnetic order

In order to check that the DFT+U can also describe correctly the magnetic ground state of UO_2, we have compared the stability of the collinear 1**k** AFM order with the experimentally observed low-temperature 3**k** AFM order [4, 80, 81]. The calculations were performed in the Jahn-Teller distorted phase, which is the one co-existing with the 3**k** AFM order. The calculations were performed in a 12-atom supercell, containing four inequivalent uranium sites, i.e. the smallest supercell enabling one to reproduce the 3**k** AFM order.

The results show that the 3**k** AFM order has approximately the same total energy as the 1**k** AFM order, with an energy difference of only 0.6 meV/UO_2. The 3**k** AFM order, however, is not obtained as the most stable one, contrary to experimental evidence. The inclusion of the spin-orbit coupling in the calculation may change this trend but its inclusion, in combination with the OMC scheme, remains challenging (see Sect. 2.4). The spin-orbit coupling was taken into account in the studies of the AFM order of UO_2 by Laskowski *et al.* [76] and Gryaznov *et al.* [21]. Laskowski *et al.* used an all-electron first-principles method and also found that the 1**k**-configuration is more stable than the 3**k** one (by around 10 meV/UO_2). On the contrary, Gryaznov *et al.* found the 3**k** AFM structure to be more stable than the 1**k**-AFM order by 95 meV/UO_2. From the distortion of the cubic lattice (c/a $<$ 1) obtained by Gryaznov *et al.*, however, it is clear that the calculations of the 1**k**-AFM order did not reach the ground state (see Table 4) and thus the relative energies calculated between the magnetic phases are biased.

In our DFT+U calculations with the non-collinear 3**k** order, the cell is perfectly cubic (a=b=c), contrary to what was obtained with the collinear 1**k** order in the fluorite phase. Moreover, we find that the non-collinear 3**k** order is associated with a distortion of the oxygen sublattice with oxygen displacements of 0.09 Å in the $\langle 111 \rangle$ direction. Even if the direction of the distortion is in agreement with the experimental data [82], the magnitude of the displacements is still significantly larger than the experimental estimation of 0.014 Å. Our results, however, are in agreement with the first-principles studies by Laskowski *et al.* and Gryaznov *et al.* who found a distortion of the oxygen sublattice of 0.16 Å and 0.09 Å, respectively.

4 Oxygen point defect formation energies in UO_2

Until recently, point-defect formation energies in uranium dioxide UO_2 were a matter of debate due to the significant discrepancies between the various studies published in the literature. The authors of the previous papers [14,15,19,22,83] on point defects in UO_2 all used the same PAW method implemented in the same code (VASP), the same Dudarev DFT+U approximation and very similar calculation parameters: the cut-off energies for the plane wave basis only differ by a few tens of eV and the values of U and J are identical. Despite these similarities, significant discrepancies not consistent with the accuracy expected from DFT were observed between the various studies, as can be seen in Table 6. The differences in the formation energies can reach 2.0 eV for uranium Frenkel pairs (consisting of a vacancy and an interstitial, non-interacting) and up to 2.7 eV for the Schottky defect (consisting of an oxygen vacancy and two uranium vacancies).

The oxygen point defect and Schottky defect formation energies are calculated as follows:

Interstitial $\mathrm{I_o}$: $E^{\mathrm{F}}_{\mathrm{I_o}} = E^{\mathrm{N+1}}_{\mathrm{I_o}} - E^{\mathrm{N}}_{\mathrm{UO_2}} - \frac{1}{2}E_{\mathrm{O_2}}$,

Vacancy $\mathrm{V_o}$: $E^{\mathrm{F}}_{\mathrm{V_o}} = E^{\mathrm{N-1}}_{\mathrm{V_o}} - E^{\mathrm{N}}_{\mathrm{UO_2}} + \frac{1}{2}E_{\mathrm{O_2}}$,

Schottky defect S : $E^{\mathrm{F}}_{\mathrm{S^i}} = E^{\mathrm{N-1}}_{\mathrm{V_U}} + 2 \times E^{\mathrm{N-1}}_{\mathrm{V_O}} - 3 \times \frac{N-1}{N} \times E^{\mathrm{N}}_{\mathrm{UO_2}}$,

Oxygen Frenkel pair $\mathrm{FP_o}$: $E^{\mathrm{F}}_{\mathrm{FP_o}} = E^{\mathrm{N-1}}_{\mathrm{V_o}} + E^{\mathrm{N+1}}_{\mathrm{I_o}}$,

where N is the number of atoms in the defect-free supercell, here $N = 96$. $E^{\mathrm{N}}_{\mathrm{UO_2}}$ is the total energy of the defect-free supercell, $E^{\mathrm{N+1}}_{\mathrm{I_o}}$ and $E^{\mathrm{N-1}}_{\mathrm{V_o}}$ the energies of the supercell containing an

Table 6: Formation energies (eV) of point defects in uranium dioxide calculated using DFT+U. The reference states used for the uranium and oxygen atoms are also indicated.

Author	References		I_o	I_u	V_o	V_u	FP_o	FP_u	S
	Uranium	Oxygen							
Iwasawa [14]	U_α (DFT+U)	$O_{2(g)}$	$-0,4$	$4,7$	$4,5$	$8,4$	$4,1$	$13,1$	$--$
Gupta [15]	–	$O_{2(g)}$	$-1,6$	$8,2$	$5,6$	$6,0$	$4,0$	$14,2$	$7,2$
Nerikar [19]	U_α	$O_{2(g)}$	$-1,3$	$6,1$	$5,3$	$9,0$	$4,0$	$15,1$	$7,6$
Yu [22]	U_α (DFT+U)	$O_{2(g)}$	$-2,4$	$2,5$	$5,1$	$4,5$	$2,6$	$7,0$	$3,6$
Tiwary [83]	–	–	$--$	$--$	$--$	$--$	$3,9$	$10,1$	$7,4$

interstitial and a vacancy, respectively. $\frac{1}{2}E_{O_2}$ is the energy by atom of the di-oxygen molecule in its triplet state, taken as the reference. The uranium point defect energies are calculated using the equivalent expressions for uranium. The point defect calculations are performed keeping the supercells neutral, but allowing for local charge redistribution inside the supercell in order to balance the presence of the defects.

For extrinsic point defects (vacancies and interstitials), formation energies are not always calculated using the same reference energy. This impacts the formation energies and may be the cause of some discrepancies. For intrinsic point defects (Frenkel pairs and Schottky defects), however, reference energies do not come into play. As a result, any discrepancy in the formation energies of such defects, as reported in Table 6, is likely due to the occurrence of metastable states.

4.1 Formation energies of oxygen point defects in the fluorite and the JT structures of UO_2

For point defect calculations, we first imposed on each uranium atom the electronic occupancies obtained for the perfect fluorite structure, as is usually done when modelling perfect UO_2. In doing so, however, the system did not relax into the lowest energy state but was trapped in a state in which the U^{4+} oxidation state of all uranium ions was preserved. To reach the lowest energy state, it was required to impose the presence of U^{5+} or U^{3+} cations in the supercell, depending on the defect modelled. Note that several charge states were considered for uranium atoms and that U^{5+} (respectively U^{3+}) ions were found to yield the lowest total energies when an oxygen interstitial (respectively vacancy) was incorporated into the system.

In both the fluorite and Jahn-Teller distorted phases, we observed two U^{5+} or two U^{3+} cations in presence of an oxygen interstitial or of an oxygen vacancy, respectively. In the case of the oxygen interstitial, we performed several additional calculations to determine the most stable location of U^{5+} cations and found it to be the second coordination sphere of the extra interstitial oxygen atom. The optimal separation distance between the two U^{5+} cations is d = 9.64 Å in the presence of the oxygen interstitial. The magnetic moments of these two cations changed from $\pm 2\mu_B$ to $\pm 1\mu_B$, suggesting the loss of one electron. By contrast, in the presence of an oxygen vacancy, the U^{3+} cations are found to be in the first coordination sphere of the missing oxygen

Figure 2: Optimized final configuration of the defective supercell containing an oxygen vacancy (left) and interstitial (right). The point defects are in yellow. Also represented (in green) are the most favourable positions for U^{3+} (left) and U^{5+} (right) cations created by charge compensation reasons. Pink spheres represent oxygen atoms that were significantly displaced from their fluorite positions.

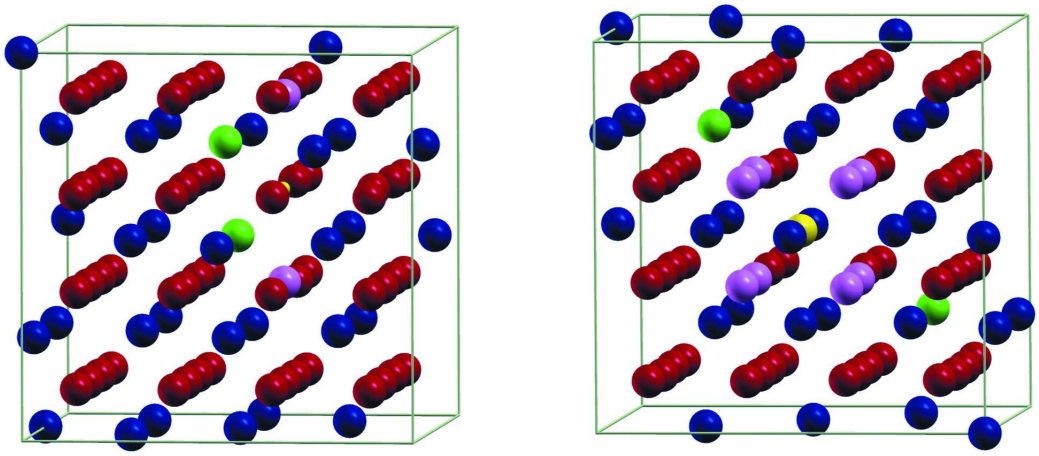

atom (see Fig. (2)).

Table 7: Formation energies (eV) of oxygen point defects (interstitial, vacancy and Frenkel pair) in uranium dioxide calculated using DFT+U, in the fluorite and the JT structure of UO_2.

	E^{F}_{Io} (eV)	E^{F}_{Vo} (eV)	E^{F}_{FPo} (eV)
Fluorite (with OM_F)	-0.05	5.30	5.25
Jahn-Teller (with OM_{JT})	0.47	6.01	6.48

Table 7 reports the formation energies of the oxygen interstitial, vacancy and Frenkel pair in both the fluorite and the JT distorted structures. For the oxygen interstitial, it can be seen that the formation energy is almost zero in the fluorite phase and 0.47 eV in the JT phase. Both these energies are small and the question of the sign of the oxygen interstitial formation energy is still a matter of debate. It seems consistent, however, to find a positive formation energy for the Jahn-Teller distorted UO_{2+x} phase given that this hyperstoichiometric phase is not stable at 0 K [84]. As for the fluorite structure, the near zero value seems surprisingly high given that UO_2 is known to oxidize easily. The DFT+U approximation, however, is not likely the cause for such a high formation energy. It is rather because of the GGA-PBE functional that fails to accurately describe the O atom and the O_2 molecule, resulting in a calculated O_2 dissociation energy that is off by 30%, 20% of which is due to the PBE functional. If we correct our value to exactly reproduce the experimental dissociation energy, the formation energy becomes -0.7 eV for the oxygen interstitial.

In both the fluorite and the Jahn-Teller distorted structures, oxygen interstitials induce a decrease of the distance between neighbouring uranium atoms, resulting in a local decrease in the cell parameters. This is in agreement with experimental observations that the cell parameters

decrease with the addition of oxygen in the material [85].

For the oxygen vacancy, the formation energies are similar in the fluorite structure (5.30 eV) and the Jahn-Teller distorted structure (6.01 eV). As regards the atomic displacements of the defect nearest neighbours, we found that the oxygen vacancy only triggers slight modifications in the bonding distances (less than 0.05 Å). As a consequence, the cell parameters remain unchanged with and without the defect.

For both oxygen interstitials and vacancies, the above results seem to show that the crystal field in UO_2 has only a moderate influence on the formation energies.

The Frenkel pair formation energy determined from neutron scattering experiments is estimated at 4.5 ± 0.5 eV, [86] which also compares well with our value of 5.25 eV calculated in the fluorite phase. Note that these energy values constitute a marked improvement over what standard DFT calculations have provided us with in the past.

DFT+U thus enables us to better apprehend the formation of point defects in UO_2 and its association with OMC scheme enables not only to circumvent the issue of metastable states but also provide us a simple procedure to treat the change of valence of the cations induced by the presence of point defects.

5 Oxygen migration energies in UO_2

The migration paths of oxygen defects were calculated using the Climbing-Image Nudged Elastic Band method (CI-NEB) [70]. This method enables one to determine the minimum energy path of an atom between two equilibrium positions in the chosen migration direction by calculating the forces acting on the migrating atom. The relaxation of the positions of the remaining atoms of the system is also taken into account. In our calculation, the forces were computed using the DFT+U framework associated with the OMC scheme, as described before. The total energy of the system is calculated for various intermediary migration steps and the migration energy is defined as the energy barrier (or saddle point) along the migration path. In this study, we considered the migration of vacancy and interstitial atoms with the migration mechanisms as follows:

• Two vacancy mechanisms, in which an oxygen atom moves to a nearest neighbour oxygen vacancy, along the <100> or the <110> direction.

• An interstitial mechanism, in which an interstitial atom in an octahedral site moves to the next nearest octahedral interstitial site.

• An indirect interstitial mechanism (interstitialcy mechanism), in which an atom in an octahedral site replaces an oxygen atom on a lattice site, which in turn moves to an octahedral interstitial site (see Fig. 3).

In order to be able to compare our results to experimental activation energies of diffusion, the calculations have been performed in the fluorite phase of UO_2. An important problem to consider for the migration calculations is the existence at 0 K of the Jahn-Teller UO_2 phase, more stable and less symmetric than the fluorite phase. This has important consequences in the CI-NEB calculations. When an atom migrates through the lattice, it breaks all symmetries

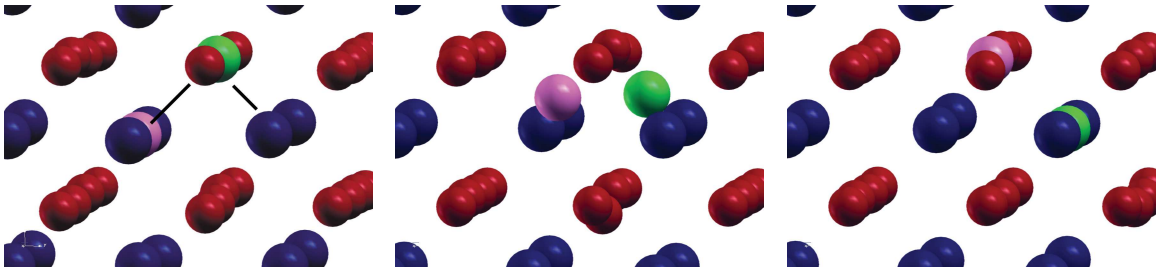

Figure 3: Minimum energy path of the interstitialcy (indirect) mechanism for oxygen self-diffusion in UO_2, calculated using DFT + U. The initial interstitial oxygen atom is in pink. The displaced oxygen lattice atom is in green.

along its trajectory. When symmetries are broken in a DFT+U calculation of UO_2 , the ground state is easier to reach but the fluorite structure tends to change back toward the Jahn-Teller distorted phase (see Sect. 3.2 and Ref. [35]). It results in a low total energy for the nonsymmetric saddle point compared to the symmetric initial and final (fluorite) configurations of the CI-NEB calculation. This constitutes a possible source of error in the determination of the migration barrier. To overcome this difficulty, it is necessary to calculate the total energy of the initial and final configurations in a very specific way, namely by performing a complete relaxation of the second and second-to-last intermediate images.

Figures 4 and 5 present the total energy curves obtained for oxygen self-diffusion via interstitial and vacancy mechanisms, respectively. It is important to emphasize that in these curves the total energy difference between an image and its symmetrical image is very small. Such a result was not *a priori* guaranteed given the large number of metastable states in the system. It emphasizes once again that the careful control of the electronic occupancies constitutes an efficient means of obtaining reliable DFT + U energies.

The <110> vacancy mechanism differs from the four other mechanisms in the sense that the associated migration path is not linear as initially envisaged. The oxygen atom first migrates toward nearby uranium atoms before moving into the oxygen vacancy. This deviation from the initial linear path is due to the Coulomb repulsion between surrounding oxygen atoms located in the same plane.

In Table 8 we report the formation and migration energies obtained from DFT+U calculations, as well as the activation energy for oxygen diffusion. The activation energy is defined according to the experimental approach detailled in Ref. [87] as the sum of the oxygen interstitial formation and migration energies. It should be stressed that the formation energy of the oxygen interstitial that we calculated in Sect. 4.1, i.e. -0.7 eV, must be corrected in order to calculate the activation energy. Indeed, this formation energy is defined as the energy required to add an oxygen atom in perfect UO_2, along with the creation of two U^{5+} cations for charge compensation. The point defect model [87] used to calculate the activation energy, however, requires the U^{5+} cations to be far from the oxygen interstitial, thus non interacting. It is therefore necessary to add to our -0.7 eV value the binding energy of two holes with the oxygen interstitial, which was evaluated to be 0.4 eV using charged supercell calculations. The oxygen interstitial formation energy with unbound U^{5+} is therefore -0.3 eV, as shown in Table 8.

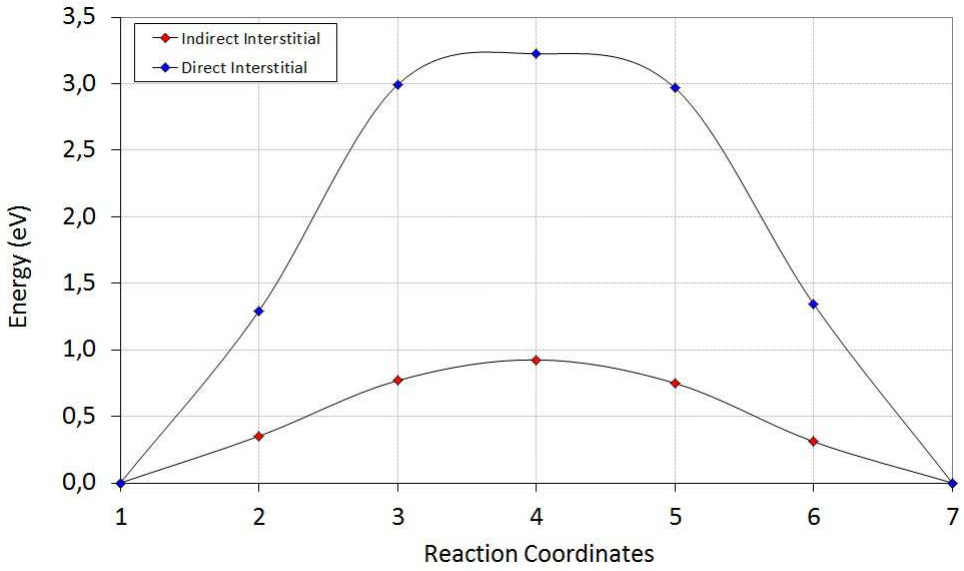

Figure 4: Total energy curve for oxygen self-diffusion in UO_2 via interstitial mechanisms (direct and indirect), calculated within the DFT + U approximation.

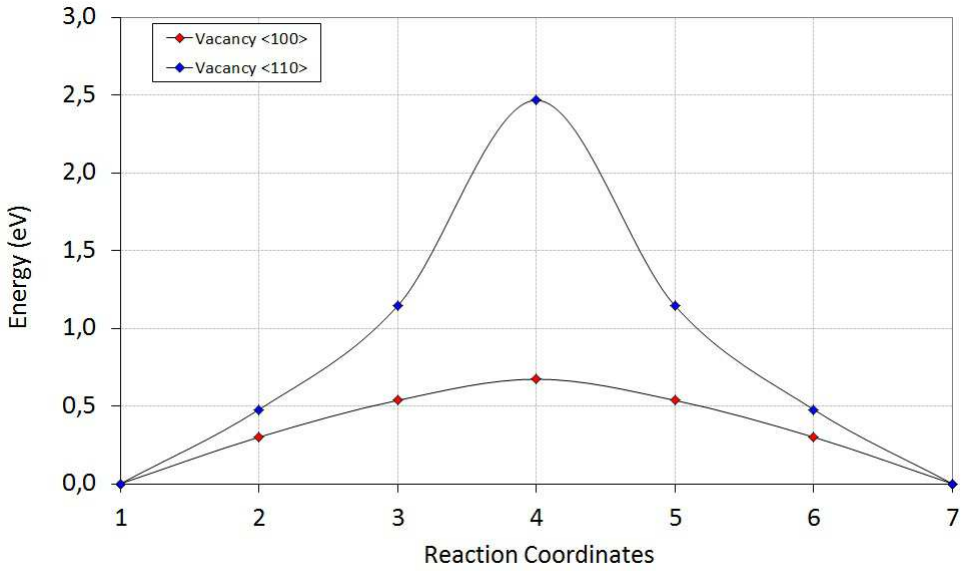

Figure 5: Total energy curve for oxygen self-diffusion in UO_2 via vacancy mechanisms (along the <100> and the <110> directions), calculated within the DFT + U approximation.

Table 8: Oxygen interstitial and vacancy formation and migration energies (in eV) calculated using the Liechtenstein DFT+U. For the oxygen interstitial mechanism, the activation energy can be compared with the experimental value.

	Formation energies (eV)	Migration energies (eV)	Activation energies (eV)
Direct	-0.30	3.22	2.92
Interstitialcy	-0.30	0.93	0.63
Vacancy <100>	5.30	0.67	/
Vacancy <110>	5.30	2.47	/

We see from Table 8 that the lowest migration energies are obtained for the interstitialcy and the vacancy <100> mechanisms, with migration energies of 0.93 and 0.67 eV, respectively. Standard DFT calculations already predicted these two mechanisms to be the most favorable [88] but quantitatively the migration energies are, however, significantly different. In particular, the migration energy for the vacancy <100> mechanism is twice lower with DFT+U (0.67 eV) than it is with standard DFT (1.2 eV). It can be also noted that the DFT+U values for the migration energies reported in Table 8 differ significantly from the ones calculated in Ref. [89] with the same DFT+U approach. In the latter study, the authors report a large negative (unphysical) value for the migration barrier associated with the oxygen interstitialcy mechanism. The main source of deviation from our results is probably that they did not control the $5f$ electronic occupancies in order to overcome the difficulties related to the presence of metastable states: the saddle-point calculation, which is less symmetric and therefore reaches the ground state more easily, has converged to a low energy state, while the initial symmetric configuration reached a higher energy metastable state.

From Table 8 we also see that the calculated DFT+U activation energies for the direct and interstitialcy mechanisms are 2.92 and 0.63 eV, respectively. The activation energy relative to the interstitialcy mechanism compares very favorably with the activation energy found experimentally [87] for oxygen diffusion (0.75 ± 0.08 eV) indicating that the interstitialcy mechanism is indeed the most probable migration mechanism, as found in other fluorite systems. The experimental work consisted in combinining tracer diffusion coefficient and electrical conductivity measurements carried out at different oxygen potentials and temperatures on UO_2 samples that contained different impurity levels. These experiments point to an oxygen migration being due to isolated oxygen interstitials over a wide range of oxygen potential. It also sheds some light on the discrepancies observed in oxygen diffusion coefficients reported previously. It is the combination of such experimental work and accurate first-principles DFT+U calculations that can provide a means of identifying the details of the migration mechanism in UO_2. Finally, our calculations can also be compared to vacancy migration values suggested from diffusion coefficient measurements in UO_{2-x} . Kim and Olander's work [90] provides us with a value of 0.5 ± 0.1 eV compared to the theoretical value of 0.67 eV.

6 Conclusion

We report here an encouraging correspondence between experimentally determined oxygen point defect formation and migration energies and those calculated from first-principles using the DFT+U approximation. We focus on the local energy minima issue that significantly affects DFT+U calculations (but also hybrid functionals calculations) for f-compounds. Calculation results were compared against a comprehensive range of experimental data involving interstitial and vacancy migration energies, and Frenkel pair formation energies. This study strongly points out that DFT+U calculations associated with electronic occupancy control, quantitatively describe oxygen transport phenomena in uranium dioxide. We also show that the fluorite structure is not the most stable phase at 0 K, as seen experimentally. The most stable phase is a Jahn-Teller distorted structure that exhibits a distortion of the oxygen cage with oxygen displacements along the <111> direction, in agreement with experiments. In the specific case of

UO_2, the existence of the Jahn-Teller distortion facilitates the search of the lowest energy states due to the symmetry breaking it induces.

These results open up the prospect of using first-principles DFT+U calculations as part of a predictive approach to determining transport properties in other actinide oxides. We are now further focusing on fission product diffusion, in particular xenon and krypton. In line with recent studies [23, 41, 91], different charge states for the defects will also be taken into account.

The future challenges for the modelling of radiation damage in UO_2 will consist in using the DFT+DMFT method (DFT+dynamical mean field theory) [32] and using recent non-local correlation functionals for van der Waals interaction. In particular, the DFT+DMFT method not only allows a better treatment of the $5f$ electron correlations, but also largely removes the problem of the local energy minima [92]. It would also enable the modelling of the paramagnetism of UO_2 above the Néel temperature. The non-local correlation functionals, such as VdW-DF (van der Waals density functional) [93, 94], will improve the description of rare gas fission products in nuclear materials.

7 Acknowledgements

This work was funded by the MATAV Nuclear Ceramics Basic Research Program. It was partly supported by the European Commission through the FP7 F-BRIDGE project (Contract No. 211690). Calculations were performed using French HPC resources available at TGCC and CINES under the allocation made by GENCI (Grand Equipement National de Calcul Intensif). David A. Andersson, Christopher R. Stanek, Blas P. Uberuaga (Los Alamos National Laboratory, USA), F. Bottin, M. Torrent, F. Jollet and Jean-Paul Crocombette (CEA) are gratefully acknowledged for discussions and collaborations on related studies.

References

[1] J. Bell. Oxygen and uranium diffusion in uranium dioxide (a review). *J. Nucl. Mater.*, 30:3, 1969.

[2] J. C. Killeen. The effect of niobium oxide additions on the electrical conductivity of UO_2. *J. Nucl. Mater.*, 88:185, 1980.

[3] G. Amoretti, A. Blaise, R. Caciuffo, J. M. Fournier, M. T. Hutchings, R. Osborn, and A. D. Taylor. 5f-electron states in uranium dioxide investigated using high-resolution neutron spectroscopy. *Phys. Rev. B*, 40:1856, 1989.

[4] R. Caciuffo, G. Amoretti, P. Santini, G. H. Lander, J. Kulda, and P. de V. Du Plessis. Magnetic excitations and dynamical Jahn-Teller distortions in UO_2. *Phys. Rev. B*, 59:13892, 1999.

[5] S. D. Conradson, D. Manara, F. Wastin, D. L. Clark, G. H. Lander, L. A. Morales, J. Rebizant, and V. V. Rondinella. Local structure and charge distribution in the UO_2-U_4O_9. *Inorg. Chem.*, 43:6922, 2004.

[6] M.-F. Barthe, H. Labrim, A. Gentils, P. Desgardin, C. Corbel, S. Esnouf, and J. P. Piron. Positron annihilation characteristics in UO_2: for lattice and vacancy defects induced by electron irradiation. *Phys. Stat. Sol. (c)*, 4:3627, 2007.

[7] P. Garcia, G. Martin, C. Sabathier, G. Carlot, A. Michel, P. Martin, B. Dorado, M. Freyss, M. Bertolus, R. Skorek, J. Noirot, L. Noirot, O. Kaitasov, and S. Maillard. Nucleation and growth of intragranular defect and insoluble atom clusters in nuclear oxide fuels. *Nucl. Instr. Meth. Phys. Res. B*, 277:98, 2012.

[8] G. Guimbretière, L. Desgranges, A. Canizares, G. Carlot, R. Caraballoand C. Jegou, F. Duval, N. Raimboux, M.R. Ammar, and P. Simon. Determination of in depth damaged profile by μ-Raman line mapping in a pre-cut irradiated UO_2. *Appl. Phys. Lett.*, 100:251914, 2012.

[9] T. Petit, C. Lemaignan, F. Jollet, B. Bigot, and A. Pasturel. Point defects in uranium dioxide. *Phil. Mag. B*, 77:779, 1998.

[10] J. P. Crocombette, F. Jollet, L. Thien, and T. Petit. Plane-wave pseudopotential study of point defects in uranium dioxide. *Phys. Rev. B*, 64:104107, 2001.

[11] M. Freyss, T. Petit, and Jean-Paul Crocombette. Point defects in uranium dioxide: Ab initio pseudopotential approach in the generalized gradient approximation. *J. Nucl. Mater.*, 347:44, 2005.

[12] K. N. Kudin, G. E. Scuseria, and R. L. Martin. Hybrid density-functional theory and the insulating gap of UO_2. *Phys. Rev. Lett.*, 89:266402, 2002.

[13] Y. Yun, H. Kim, H. Kim, and K. Park. Ab initio calculations of strongly correlated electrons: antiferromagnetic ground state of UO_2. *Nucl. Eng. and Tech.*, 37:293, 2005.

[14] M. Iwasawa, Y. Chen, Y. Kaneta, T. Ohnuma, H.-Y. Geng, and M. Kinoshita. First-principles calculations of point defects in uranium dioxide. *Mater. Trans.*, 47:2651, 2006.

[15] F. Gupta, G. Brillant, and A. Pasturel. Correlation effects and energetics of point defects in uranium dioxide : A first principle investigation. *Philos. Mag.*, 87:2561, 2007.

[16] L. Petit, A. Svane, Z. Szotek, W.M. Temmerman, and G.M. Stocks. Electronic structure and ionicity of actinide oxides from first principles. *Phys. Rev. B*, 81:045108, 2010.

[17] B. Dorado, B. Amadon, M. Freyss, and M. Bertolus. DFT+U calculations of the ground state and metastable states of uranium dioxide. *Phys. Rev. B*, 79:235125, 2009.

[18] I. D. Prodan, G. E. Scuseria, and R. L. Martin. Covalency in the actinide dioxides: Systematic study of the electronic properties using screened hybrid density functional theory. *Phys. Rev. B*, 76:033101, 2007.

[19] P. V. Nerikar, T. Watanabe, J. S. Tulenko, S. R. Phillpot, and S. B. Sinnott. Energetics of intrinsic point defects in uranium dioxide from electronic-structure calculations. *J. Nucl. Mater.*, 384:61, 2009.

[20] D. A. Andersson, J. Lezama, B. P. Uberuaga, C. Deo, and S. D. Conradson. Cooperativity among defect sites in AO_{2+x} and A_4O_9 (A=U,Np,Pu) : Density functional calculations. *Phys. Rev. B*, 79:024110, 2009.

[21] D. Gryaznov, E. Heifets, and D. Sedmidubsky. Density functional theory calculations on magnetic properties of actinide compounds. *Phys. Chem. Chem. Phys.*, 12:12273, 2010.

[22] J. Yu, R. Devanathan, and W. J. Weber. First-principles study of defects and phase transition in UO_2. *J. Phys. : Condens. Matter*, 21:435401, 2009.

[23] J. P. Crocombette. Influence of charge states on energies of point defects and clusters in uranium dioxide. *Phys. Rev. B*, 85:144101, 2012.

[24] P. Hohenberg and W. Kohn. Inhomogeneous electron gas. *Phys. Rev.*, 136:B864, 1964.

[25] W. Kohn and L.J. Sham. Self-consistent equations including exchange and correlation effects. *Phys. Rev.*, 140:A1133, 1965.

[26] J. Heyd, G. E. Scuseria, and M. Ernzerhof. Hybrid functionals based on a screened Coulomb potential. *J. Chem. Phys.*, 118:8207, 2003.

[27] C. Adamo and V. Barone. Toward reliable density functional methods without adjustable parameters: The PBE0 mode. *J. Chem. Phys.*, 110:6158, 1999.

[28] L. Petit, A. Svane, Z. Szotek, and W.M. Temmerman. First-principles calculations on $PuO_{2\pm x}$. *Science*, 301:498, 2003.

[29] V. I. Anisimov, J. Zaanen, and O. K. Andersen. Band theory and Mott insulators: Hubbard U instead of Stoner I. *Phys. Rev. B*, 44:943, 1991.

[30] A. I. Liechtenstein and J. Zaanen V. I. Anisimov. Density-functional theory and strong interactions : Orbital ordering in Mott-Hubbard insulators. *Phys. Rev. B*, 52:R5467, 1995.

[31] S. L. Dudarev, G. A. Botton, S. Y. Savrasov, C. J. Humphreys, and A. P. Sutton. Energy-loss spectra and the structural stability of nickel oxide - an LSDA+U study. *Phys. Rev. B*, 57:1505, 1998.

[32] A. Georges, G. Kotliar, and W. Krauth annd M. J. Rozenberg. Dynamical mean-field theory of strongly correlated fermion systems and the limit of infinite dimensions. *Rev. Mod. Phys*, 68:13, 1996.

[33] G. Kotliar, S. Y. Savrasov, K. Haule, V. S. Oudovenko, O. Parcollet, and C. A. Marianetti. Electronic structure calculations with dynamical mean-field theory. *Rev. Mod. Phys*, 78:865, 2006.

[34] D. A. Andersson, T. Watanabe, C. Deo, and B. P. Uberuaga. Role of di-interstitial clusters in oxygen transport in UO_{2+x} from first principles. *Phys. Rev. B*, 80:060101, 2009.

[35] B. Dorado, G. Jomard, M. Freyss, and M. Bertolus. Stability of oxygen point defects in UO_2 by first-principles DFT+U calculations: Occupation matrix control and Jahn-Teller distortion. *Phys. Rev. B*, 82:035114, 2010.

[36] F. Jollet, G. Jomard, B. Amadon, J.P. Crocombette, and D. Torumba. Hybrid functional for correlated electrons in the projector augmented-wave formalism: Study of multiple minima for actinide oxides. *Phys. Rev. B*, 80:235109, 2009.

[37] P. V. Nerikar, X.-Y. Liu, B. P. Uberuaga, C. R. Stanek, S. R. Phillpot, and S. B. Sinnott. Thermodynamics of fission products in $UO_{2\pm x}$. *J. Phys. : Condens. Matter*, 21:435602, 2009.

[38] B. Dorado, M. Freyss, and G. Martin. An atomistic approach to self-diffusion in uranium dioxide. *Eur. Phys. J. B*, 69:230, 2009.

[39] G. Brillant and A. Pasturel. Study of Ba and Zr stability in $UO_{2\pm x}$ by density functional calculations. *Phys. Rev. B*, 77:184110, 2008.

[40] G. Brillant, F. Gupta, and A. Pasturel. Investigation of molybdenum and caesium behaviour in urania by ab initio calculations. *J. Phys. : Condens. Matter*, 21:285602, 2009.

[41] D. A. Andersson, B. P. Uberuaga, P. V. Nerikar, C. Unal, and C. R. Stanek. U and Xe transport in $UO_{2\pm x}$: Density functional theory calculations. *Phys. Rev. B*, 84:054105, 2011.

[42] Y. Yun, O. Eriksson, and P. M. Oppeneer. Theory of he trapping, diffusion, and clustering in UO_2. *J. Nucl. Mater.*, 385:510, 2009.

[43] D. Gryaznov, E. Heifets, and E. Kotomin. Ab initio DFT+U study of he atom incorporation into UO_2 crystals. *Phys. Chem. Chem. Phys.*, 11:7241, 2009.

[44] W. H. Adams. Stability of Hartree-Fock states. *Phys. Rev.*, 127:1650, 1962.

[45] H. Fukutome. Unrestricted Hartree-Fock theory and its applications to molecules and chemical reactions. *International Journal of Quantum Chemistry*, 20:955, 1981.

[46] A. B. Shick, W. E. Pickett, and A. I. Lichtenstein. Ground and mestastable states in γ-Ce from correlated band theory. *J. Electron Spectrosc. Relat. Phenom.*, 114-116:753, 2001.

[47] B. Amadon, F. Jollet, and M. Torrent. γ and β cerium: LDA + U calculations of ground-state parameters. *Phys. Rev. B*, 77:155104, 2008.

[48] F. Tran, J. Schweifer, P. Blaha, K. Schwarz, and P. Novák. PBE+U calculations of the Jahn-Teller effect in PrO_2. *Phys. Rev. B*, 77:085123, 2008.

[49] G. Jomard, B. Amadon, F. Bottin, and M. Torrent. Structural, thermodynamic, and electronic properties of plutonium oxides from first principles. *Phys. Rev. B*, 78:075125, 2008.

[50] P. Larson, W.R.L. Lambrecht, A. Chantis, and M. van Schilfgaarde. Electronic structure of rare-earth nitrides using the LSDA+U approach: Importance of allowing $4f$ orbitals to break the cubic crystal symmetry. *Phys. Rev. B*, 75:045114, 2007.

[51] B. Meredig, A. Thompsonand H. A. Hansen., C. Wolverton, and A. van de Walle. Method for locating low-energy solutions within DFT+U. *Phys. Rev. B*, 82:195128, 2010.

[52] H. Y. Geng, Y. Chen, Y. Kaneta, M. Kinoshita, and Q. Wu. Interplay of defect cluster and the stability of xenon in uranium dioxide from density functional calculations. *Phys. Rev. B*, 82:094106, 2010.

[53] J. Hubbard. Electron correlations in narrown energy bands. iv. atomic representation. *Proc. R. Soc. Lond. A*, 285:542, 1965.

[54] E. R. Ylvisaker, W. E. Pickett, and K. Koepernik. Anisotropy and magnetism in the LSDA+U method. *Phys. Rev. B*, 79:035103, 2009.

[55] M. T. Czyżyk and G. A. Sawatzky. Local-density functional and on-site correlations : The electronic structure of La_2CuO_4 and $LaCuO_3$. *Phys. Rev. B*, 49:14211, 1994.

[56] V. I. Anisimov, F. Aryasetiawan, and A. I. Lichtenstein. Electronic structure and spectra of strongly correlated systems : the LDA+U method. *J. Phys. : Condens. Matter*, 9:767, 1997.

[57] M. Cococcioni and S. de Gironcoli. Linear response approach to the calculation of the effective interaction parameters in the LDA + U method. *Phys. Rev. B*, 71:035105, 2005.

[58] P. O. Lowdin. Discussion on the Hartree-Fock approximation. *Rev. Mod. Phys.*, 35:496, 1963.

[59] A.J. Devey. First principles calculation of the elastic constants and phonon modes of UO_2 using GGA + U with orbital occupancy control. *J. Nucl. Mater.*, 412:301, 2011.

[60] A.E. Thompson and C. Wolverton. First-principles study of noble gas impurities and defects in UO_2. *Phys. Rev. B*, 84:134111, 2011.

[61] B. Dorado, B. Amadon, G. Jomard, M. Freyss, and M. Bertolus. Comment on "interplay of defect cluster and the stability of xenon in uranium dioxide from density functional calculations". *Phys. Rev. B*, 84:096101, 2011.

[62] *http://www.abinit.org.*

[63] P. E. Blöchl. Projector augmented-wave method. *Phys. Rev. B*, 50:17953, 1994.

[64] http://cms.mpi.univie.ac.at/vasp/.

[65] J. Hafner. Ab initio simulations of materials using VASP: Density functional theory and beyond. *J. Comput. Chem.*, 29:2044, 2008.

[66] X. Gonze, B. Amadon, P.-M. Anglade, J.-M. Beuken, F. Bottin, P. Boulanger, D. Caliste F. Bruneval, M. Côté R. Caracas, T. Deutsch, L. Genovese, P. Ghosez, M. Giantomassi, S. Goedecker, D. R. Hamann, P. Hermet, F. Jollet, G. Jomard, S. Leroux, M. Mancini, S. Mazevet, M. J. T. Oliveira, G. Onida, Y. Pouillon, T. Rangel, G.-M. Rignanese, D. Sangalli, R. Shaltaf, M. Torrent, M. J. Verstraete, G. Zerah, and J. Zwanziger. Abinit : First-principles approach to material and nanosystem properties. *Comput. Phys. Commun.*, 180:2582, 2009.

[67] J. P. Perdew, S. Burke, and M. Ernzerhof. Generalized gradient approximation made simple. *Phys. Rev. Lett.*, 77:3865, 1996.

[68] T. Yamazaki and A. Kotan. Systematic analysis of 4f core photoemission spectra in actinide oxides. *J. Phys. Soc. Jpn.*, 60:49, 1991.

[69] A. Kotani and T. Yamazaki. Systematic analysis of core photoemission spectra for actinide di-oxides and rare-earth sesqui-oxides. *Prog. Theor. Phys.*, 108:117, 1992.

[70] G. Henkelman, B. P. Uberuaga, and H. Jonsson. A climbing image nudged elastic band method for finding saddle points and minimum energy paths. *J. Chem. Phys.*, 113:9901, 2000.

[71] D. Ippolito, L. Martinelli, and G. Bevilacqua. Dynamical Jahn-Teller effect on UO_2. *Phys. Rev. B*, 71:064419, 2005.

[72] E. Blackburn, R. Caciuffo, N. Magnani, P. Santini, P. J. Brown, M. Enderle, and G. H. Lander. Spherical neutron spin polarimetry of anisotropic magnetic fluctuations in UO_2. *Phys. Rev. B*, 72:184411, 2005.

[73] S. B. Wilkins, R. Caciuffo, C. Detlefs, J. Rebizant, E. Colineau, F. Wastin, and G. H. Lander. Direct observation of electric-quadrupolar order in UO_2. *Phys. Rev. B*, 73:060406(R), 2006.

[74] P. Santini, S. Carretta, G. Amoretti, R. Caciuffo, N. Magnani, and G. H. Lander. Multipolar interactions in f-electron systems: The paradigm of actinide dioxides. *Rev. Mod. Phys*, 81:807, 2009.

[75] P. Santini, Romuald Lemanski, and Paul Erdos. Magnetism of actinide compounds. *Adv. Phys*, 48:537, 1999.

[76] R. Laskowski, G. K. H. Madsen, P. Blaha, and K. Schwarz. Magnetic structure and electric-field gradients of uranium dioxide : an ab initio study. *Phys. Rev. B*, 69:140408R, 2004.

[77] I. J. Fritz. Elastic properties of UO_2 at high pressure. *J. Appl. Phys.*, 352:4353, 1976.

[78] M. Idiri, T. LeBihan, S. Heathman, and J. Rebizant. Behavior of actinide dioxides under pressure: UO_2 and ThO_2. *Phys. Rev. B*, 70:014113, 2004.

[79] O. G. Brandt and C. T. Walker. Temperature dependence of elastic constants and thermal expansion for UO_2. *Phys. Rev. Lett.*, 18:11, 1967.

[80] J. Faber, G. H. Lander, and B. R. Cooper. Neutron-diffraction study of UO_2 : Observation of an internal distortion. *J. Phys. Chem.*, 35:1770, 1975.

[81] P. Burlet, J. Rossat-Mignod, S. Vuevel, O. Vogt, J. C. Spirlet, and J. Rebivant. Neutron diffraction on actinides. *J. Less-Common Met.*, 121:121, 1986.

[82] K. Ikushima, S. Tsutsui, Y. Haga, H. Yasuoka, R. E. Walstedt, N. M. Masaki, A. Nakamura, S. Nasu, and Y. Onuki. First-order transition in UO_2 : ^{235}U and ^{17}O NMR study. *Phys. Rev. B*, 63:104404, 2001.

[83] P. Tiwary, A. van de Walle, and N. Grønbech-Jensen. *Ab initio* construction of interatomic potentials for uranium dioxide across all interatomic distances. *Phys. Rev. B*, 80:174302, 2009.

[84] J. Higgs, W. T. Thompson, B. J. Lewis, and S. C. Vogel. Kinetics of precipitation of U_4O_9 from hyperstoichiometric UO_{2+x}. *J. Nucl. Mater.*, 366:297, 2007.

[85] K. Teske, H. Ullmann, and D. Rettig. Investigation of the oxygen activity of oxide fuels and fuel-fission product systems by solid electrolyte techniques. part i: Qualification and limitations of the method. *J. Nucl. Mater.*, 116:260, 1983.

[86] K. Clausen, W. Hayes, J. E. Macdonald, R. Osborn, and M. T. Hutchings. Observation of oxygen Frenkel disorder in uranium dioxide above 2000 K by use of neutron-scattering techniques. *Phys. Rev. Lett.*, 52:1238, 1984.

[87] B. Dorado, P. Garcia, G. Carlot, C. Davoisne, M. Fraczkiewicz, B. Pasquet, M. Freyss, C. Valot, G. Baldinozzi, D. Siméone, and M. Bertolus. First-principles calculation and experimental study of oxygen diffusion in uranium dioxide. *Phys. Rev. B*, 83:035126, 2011.

[88] B. Dorado, J. Durinck, P. Garcia, M. Freyss, and M. Bertolus. An atomistic approach to self-diffusion in uranium dioxide. *J. Nucl. Mater.*, 400:103, 2009.

[89] F. Gupta, A. Pasturel, and G. Brillant. Diffusion of oxygen in uranium dioxide: A first-principles investigation. *Phys. Rev. B.*, 81:014110, 2010.

[90] K. Kim and D. Olander. Oxygen diffusion in UO_{2-x}. *J. Nucl. Mater.*, 102:192, 1981.

[91] J. P. Crocombette, D. Torumba, and A. Chartier. Charge states of point defects in uranium oxide calculated with a local hybrid functional for correlated electrons. *Phys. Rev. B*, 83:184107, 2011.

[92] B. Amadon. A self-consistent DFT + DMFT scheme in the projector augmented wave method: applications to cerium, Ce_2O_3 and Pu_2O_3 with the Hubbard I solver and comparison to DFT+U. *J. Phys. Condens. Matter*, 24:075604, 2012.

[93] M. Dion, H. Rydberg, E. Schröder, D. C. Langreth, and B. I. Lundqvist. Van der Waals density functional for general geometries. *Phys. Rev. Lett.*, 92:246401, 2004.

[94] C. Espejo, T. Rangel, Y. Pouillon, A.H. Romero, and X. Gonze. Wannier functions approach to Van der Waals interactions in ABINIT. *Comp. Phys. Comm.*, 183:480, 2012.